Proceedings of ASME Turbo Expo 2008: Power for Land, Sea and Air
GT2008
June 9-13, 2008, Berlin, Germany

GT2008-50715

LOSSES IN HIGH SPEED PERMANENT MAGNET MACHINES USED IN MICROTURBINE APPLICATIONS

Co Huynh, Liping Zheng, and Dipjyoti Acharya

Calnetix, Inc., Cerritos, CA 90703 USA

ABSTRACT

High speed permanent magnet (PM) machines are used in microturbine applications due to their compactness, robust construction and high efficiency characteristics. These machines are integrated with the turbines and rotate at same speeds. This paper discusses in details losses in high speed PM machines. A typical PM machine designed for microturbine application is presented with its detailed loss calculations. Various loss verification methods are also discussed.

1 INTRODUCTION

Microturbines are small combustion turbines with typical outputs in the range of 20 kW to 500 kW. A typical system rotates over 40,000 rpm. One of the key enabling technologies for microturbines is the integral high speed electrical machines operating at same speeds as the turbines, eliminating mechanical gearboxes. The result is a very compact, high efficiency system that allows for ease of onsite installation. High speed permanent magnet (PM) machines are typically used in microturbine application due to their high power density and high efficiency characteristics. Good understanding of high speed PM machine characteristics especially its losses is critical to predict system performance and to ensure reliable operation.

Losses in PM machine can be divided into three categories: (a) stator loss; (b) rotor eddy current loss; and (c) windage loss. The stator loss consists of copper loss and iron loss. The copper loss includes conventional I^2R loss and stray load loss due to skin effect and proximity effect. This can be calculated based on finite element analysis (FEA) or using analytical methods. The stator iron loss is divided into hysteresis loss, classical eddy current loss, and excess eddy current loss. Empirical equations or time-step transient FEA with motion can be used to calculate iron loss. The rotor loss generated by induced eddy currents in the steel shaft and permanent magnets is not significant compared to the machine's total loss. However, removing the heat from rotor to ensure reasonable operating temperatures of its components is more difficult than removing the heat from the stator. Thus, accurate prediction of rotor loss becomes important especially at high speed. The major causes of the rotor loss are: (a) space harmonics due to existence of stator slot opening, and winding distribution, and (b) time harmonics of the phase currents due to pulse width modulation (PWM). The rotor loss can be analyzed using analytical methods. However, simulations using FEA based on actual measured current waveforms or estimated current with total harmonics distortion (THD) provides a more accurate assessment. The windage loss as the result of shearing action of the media that exists between the rotor and stator may also be significant at high-speed, especially with small airgap and high cooling flow pressure in the airgap between the rotor and stator.

Spin down test can be used to verify no-load loss, especially when the rotor's inertia is large. Testing of a back-to-back configuration can verify machine's efficiencies and total machine losses at various loaded conditions. Thermal analysis model result compared with measured temperatures mapping can also be used to verify machine losses.

2 PERMANENT MAGNET ALTERNATOR LOSSES

The losses in PM alternators are grouped into: (a) stator loss; (b) rotor eddy current loss; and (c) windage loss.

2.1 Stator Loss

The stator loss consists of copper loss and iron loss.

Copper Loss is the loss due to the current going through the armature windings. The copper loss consists of I^2R loss and stray load loss. The I^2R loss is given by

$$P_{cu} = m_1 I^2 R \quad (1)$$

where m_1 is the number of phases, I is the armature current, and R is the dc armature resistance. The I^2R loss can be significant when large current flows through the conductor with large ohmic resistance.

The stray loss comes from: (a) skin effect resulting from the same source conductors, and (b) proximity effect resulting from the field induced from adjacent conductors sharing the same slot.

The skin effect is caused by electromagnetic induction in the conducting material which opposes the currents set up by the wave E-field. The skin depth is the distance in which an electromagnetic wave entering a conducting surface is damped and reduces in amplitude by a factor *1/e*, where *e* is equal to 2.71828…. The skin depth (δ) is given by

$$\delta = \sqrt{\frac{2}{\omega \mu_0 \sigma}} \quad (2)$$

where ω is the angular frequency of the current and σ is the electrical conductivity of the conducting material.

In designing the stator winding, wire strand size is selected such that skin depth is much larger than the wire radius to minimize loss due to skin effect.

Stator windings are contained inside slots. Loss due to proximity effects of conductors located in the slots of electric machines can be estimated based on the following equation [1]

$$P_{stray} = P_{cu}(k_d - 1) \quad (3)$$

where

$$k_d = \phi(\xi) + \left[\frac{m^2-1}{3} - \left(\frac{m}{2}\sin\left(\frac{\gamma}{2}\right)\right)^2\right]\psi(\xi), \quad (4)$$

$$\phi(\xi) = \xi \frac{\sinh(2\xi) + \sin(2\xi)}{\cosh(2\xi) - \cos(2\xi)}, \quad (5)$$

$$\psi(\xi) = 2\xi \frac{\sinh(\xi) - \sin(\xi)}{\cosh(\xi) + \cos(\xi)}, \quad (6)$$

and ξ is the relative height of a conductor (the ratio of its height to the effective skin depth δ considering insulation). γ is the phase angle between the upper layer and lower layer currents for two-layer case, *m* is the total number of identical conductors in layers, *kd* is the average resistance coefficient, which is the ratio of effective ac resistance vs. dc resistance.

The copper loss is temperature dependent, so the copper loss is calculated at the expected copper temperature. The copper I^2R loss increases when copper temperature increases due to increased winding resistance, while the copper stray load loss reduces with increased temperature. In addition to the analytical method described above, loss due to proximity effect and skin effect can also be simulated based on transient time-stepping FEA [2]. However, this method is very time consuming especially when multiple strands are used.

Iron Loss produced in a magnetic material operating in an alternating magnetizing field is generally separated into two components: hysteresis loss, and eddy current loss.

Hysteresis loss is due to a form of intermolecular friction when a varying magnetic field is applied to the magnetic material. The loss per cycle is proportional to the area enclosed by the hysteresis loop on the B-H characteristics of the material. The hysteresis loss increases with the maximum magnetic field as is illustrated in Figure 1.

The empirical formula expressing the hysteresis loss per unit volume (P_h, W/m^3) in terms of the maximum flux density (*B*, T) and frequency (*f*, Hz) was developed by Steinmetz [3] as follows

$$P_h = \eta B^n f \quad (7)$$

where η is a material constant and *n* is an exponent which has a typical value between 1.8 and 2.2, depending on the lamination material[4].

The term "eddy current" refers to circulating electric currents that are induced in a sheet of a conducting material when it is subjected to alternating magnetic field. These eddy currents produce power that is dissipated as heat. The eddy current loss per unit volume (P_e, W/m^3), at frequencies which are low enough for the inductive effects to be neglected, is given by the general equation [3]

$$P_e = \frac{\pi^2 B^2 t^2 f^2}{\rho \beta} \quad (8)$$

where *t* is the thickness of the material (m), *B* is the peak flux density (T), ρ is the resistivity of the material (Ω·m) and β is a coefficient that is related to the geometric structure.

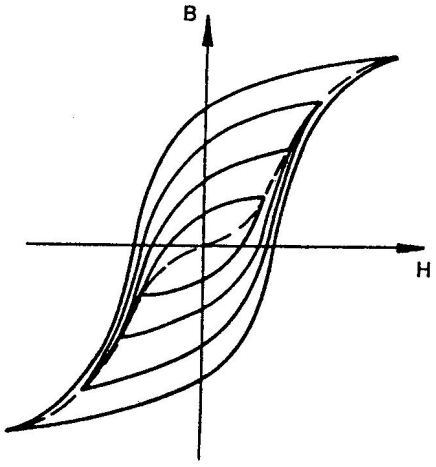

Figure 1 Family of hysteresis loops.

Eddy current loss can also be divided into classical eddy current loss and excess eddy current loss for more accurate analysis. Therefore, at a given frequency (*f*), the iron loss for electrical steel can be calculated from [5], [6]:

$$P_{iron} = k_h B^2 f + K_c (Bf)^2 + K_e (Bf)^{3/2} \qquad (9)$$

where K_h, K_c and K_e are the coefficients of hysteresis loss, classical eddy current loss, and excess eddy current loss, respectively, B is the peak flux density. The coefficients can be calculated using curve fitting of the iron loss data from manufacturers or from material test data.

The above equation is based on the assumption of sinusoidal excitation. When the iron core is subjected to nonsinusoidal magnetic field, the distorted excitation, which can be represented by higher order harmonics, has to be considered [7], [8]. The iron loss model considering arbitrary magnetic flux waveforms can be found in [9]. The transient time-stepping finite element method is also widely used to directly simulate the core loss [10], [11].

Soft magnetic materials form the magnetic circuit in an electric machine. An ideal material would have high permeability in order to reduce the reluctance of the magnetic circuit, high saturation flux density in order to minimize the volume and weight of the iron core, and low losses. However, it is impossible to optimize all of these properties in a single material. This is because there are a large number of factors that affect magnetic properties (chemical composition, mechanical treatment and thermal treatment are the most important), and the result is often a compromise. For example, nickel steel has low iron loss but low saturation flux density, while cobalt steel has higher saturation flux density but also higher iron loss. Iron core of the machine is made up of thin laminations in order to reduce core loss. Laminations as thin as 0.127 mm are generally used in high frequency applications in order to reduce iron loss.

Besides the laminated core, there are also two alternative materials [12] (a) amorphous metals (such as metglas), instead of the poly-crystalline structure, have very low hysteresis and eddy-current losses. Amorphous metals are produced by rapid cooling of alloys consisting of iron, nickel and /or cobalt together with one or more of the following metalloids which is an element or compound exhibiting both metallic and non-metallic properties: boron, silicon and carbon; and (b) powder materials (such as grain-oriented electrical steels), which, in spite of its rather low core permeance, may be attractive for very high frequency applications, and also on account of effective damping of vibrations.

2.2 Rotor Loss

The rotor loss generated by induced eddy current in the steel shaft and permanent magnets is not significant compared to the total machine loss. However, removing the heat from the rotor to ensure reasonable operating temperatures of its components is more difficult than removing the heat from the stator. Thus, accurate prediction of rotor loss becomes important especially at high-speed. The major causes of the rotor eddy current loss can be categorized into the following three groups: (a) no-load rotor eddy current loss caused by the existence of slots, (b) on-load rotor eddy current loss induced by the harmonics of windings' magnetomotive force (MMF), which is also called space harmonics, and (c) on-load rotor eddy current loss induced by the time harmonics of the phase currents due to pulse width modulation (PWM).

Loss due to eddy current in general can be expressed by

$$P = \int_V \sigma \mathbf{E}^2 dV = \int_V \mathbf{J}^2 / \sigma \, dV \qquad (10)$$

where σ is the material conductivity, **E** is the electric field, **J** is the eddy current density, and V is the volume of the material. For accurate assessment, the rotor loss is generally simulated using 2-D FEA time-stepping transient solver with motion, in which the actual measured motor/generator current waveforms are applied. For alternators with passive rectifier, 2-D FEA transient solver with motion and external circuits can be used to simulate rotor loss and alternator performance. Figure 2 shows one example of eddy currents in the rotor caused by slot effect, winding space harmonics and phase current time harmonics.

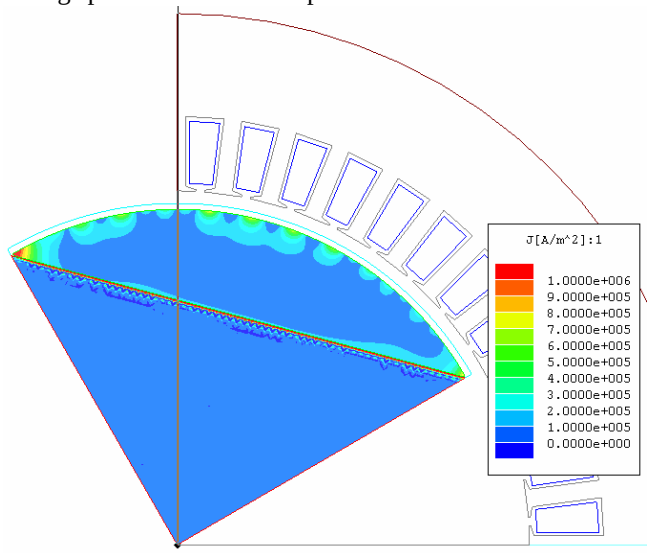

Figure 2 Eddy currents in the rotor.

There are several methods to reduce rotor eddy current losses. Reducing slot opening and increasing magnetic gap between rotor and stator can reduce no-load rotor loss. Increasing number of slots per pole and using fractional winding can reduce rotor loss caused by the space harmonics of the armature winding. Increasing switching frequency and using external line inductors can reduce rotor loss caused by time harmonics of the phase currents. Since rotor loss caused by time harmonics is dominant in most applications, increasing switching frequency and using external line inductance to

reduce current THD is a very effective way to reduce rotor loss.

2.3 Windage Loss

Windage loss is heat generated in the fluid due to relative motion (shearing) of the fluid that flows between the rotor and stator [13]. Windage loss, depending on various gases at various operating conditions, as used in high speed machines can be very high contributing to overall machine's inefficiency. The windage loss generation is a function of shaft rotational speed, fluid properties such as temperature, pressure, density, and temperature gradients at stator and rotor walls.

The windage loss generated in the clearance between a rotating cylinder and a stationary cylinder with homogenous, laminar flow (no axial flow) can be estimated from the following system of equations given by [13]

Shaft rotational speed $$\omega = \frac{2 * \pi * N}{60} \quad (11)$$

Reynolds number $$\mathrm{Re} = \omega * r * \frac{\rho}{\mu} * \phi \quad (12)$$

Skin friction coefficient (C_d) for turbulent flow is determined by

$$\frac{1}{\sqrt{C_d}} = 2.04 + 1.768 * \ln(\mathrm{Re} * \sqrt{C_d}) \quad (13)$$

Windage $$W = C_D * \pi * \rho * \omega^3 * r^4 * \lambda \quad (14)$$

where,

N = rotational speed of rotor, in revolutions per minute
ρ = density of fluid, in kg/m^3
μ = kinematic viscosity of cooling media, m^2/s
r = radius of the rotor, in m
φ = radial gap between rotor and stator, in m
λ = length of the rotor, in m

Theoretical relations and experimental validation taking into account combination of axial flow and rotational flow, in case of cooling media passing through the gap can be included to obtain a better estimate. Also, surface roughness of the stator tooth and rotor surface affects windage loss and must be taken into account [14].

3 TYPICAL ALTERNATOR DESIGN AND LOSS CALCULATION

The detailed loss breakdown of a 120 kW alternator is provided as an example. The cross section of the alternator is shown in Figure 3. Basic alternator performance parameters are shown in Table 1. The stator core is made of 0.178 mm silicon steel and the length is 162 mm. The alternator output is connected to a passive rectifier shown in Figure 4. A 2.86 Ω power resistor is used as an equivalent load to provide 120 kW output power.

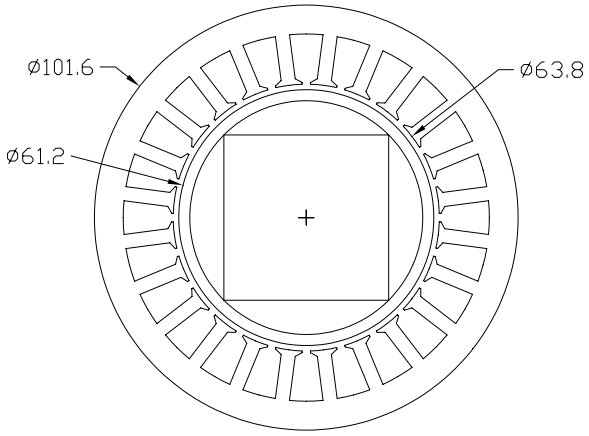

Figure 3 The cross section of a 120 kW alternator (unit is in mm).

Table 1 Parameters of the motor/generator.

Machine type	PM Synchronous
Operating speed	70,000 rpm
Number of phases	3
Number of slots	24
Number of conductor /slot	6
Number of circuits	2
Winding resistance (line-neutral)	16.3 mΩ @ 150°C (excl. leads)
Winding leakage inductance(per phase)	40 uH
D-axis magnetizing inductance (Lad)	39.3 uH
Q-axis magnetizing inductance (Laq)	54.6 uH
L-L Back EMF constant (Vrms/krpm)	8.26
Weight of core iron (kg)	2.37
Weight of teeth iron (kg)	1.20

The alternator performance was simulated using transient FEA with external circuit, and the result is summarized in Table 2. The phase current waveforms are also plotted in Figure 5.

Table 2 Simulated Performances.

Output dc voltage (V)	583.7
Output dc current (A)	204.1
Output phase current (Arms)	154.5

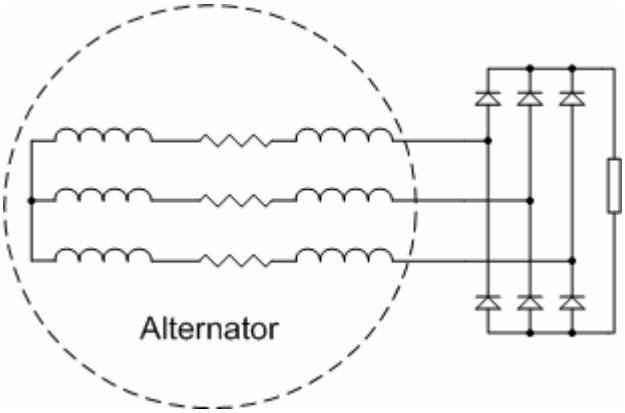

Figure 4 Passive rectifier circuits.

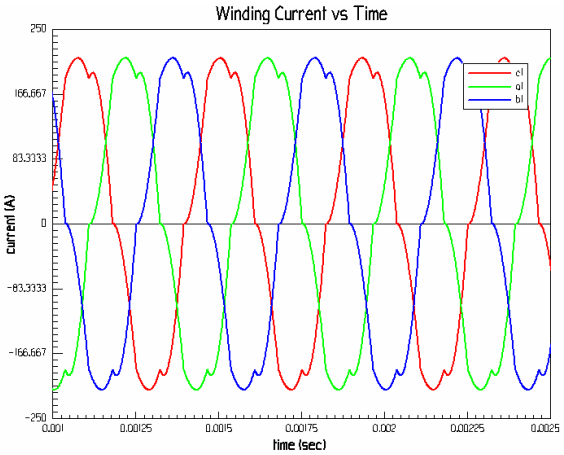

Figure 5 Simulated current waveforms.

Based on (1), the copper I^2R loss is calculated to be 1167 W. According to (4), the resistance coefficient is 1.12, so the total copper loss is 1308 W (including 141 W of copper stray load loss).

The air density at 77 °C is 1.009 kg/m^3, and the viscosity is 2.075 m^2/s. According to (11) - (14), we have Reynolds number (Re) equals to 14179, skin friction coefficient (C_d) equals to 4.928E-3, and the windage loss is calculated to be 874 Watts.

Based on curve fitting of manufacturer's data using genetic algorithm, we get the coefficients of (9) as,

$$K_h = 0.0275 \frac{W}{Hz \cdot T^2 \cdot kg} \tag{16}$$

$$K_c = 1.83E-5 \frac{W}{Hz^2 \cdot T^2 \cdot kg} \tag{17}$$

$$K_e = 0.000277 \frac{W}{Hz^{1.5} \cdot T^{1.5} \cdot kg} \tag{18}$$

According to FEA, the peak flux density is 1.45 T in the core and 1.17 T in the teeth. Therefore, according to (9), the core loss is calculated to be 945 W, and teeth loss to be 317 W.

For rotor loss, FEA simulation with motor current waveform due to passive rectifier was performed, and the rotor loss was found to be 221.9 W. The rotor loss due to current time harmonics is dominant because of high current harmonic distortions when using passive rectifier.

In summary, the losses of the high-speed alternator at rated load, excluding power electronics losses are shown in Table 3.

Table 3 Summary of losses at rated load.

Stator loss	
Copper loss (W)	1308
Iron loss (W)	1262
Rotor loss	
Shaft loss (W)	15.9
PM loss (W)	206
Windage loss (W)	874
Total loss (W)	3666
Rated output power (W)	120000
PM alternator efficiency (%)	97.0

4 VERIFICATION OF LOSSES

Various methods can be used to verify alternator losses and operating efficiency.

4.1 Back-to-Back Test

For high speed machines, back-to-back test configuration is most widely used to map machines performance at various load conditions from no load to full load. In this test, two identical machines are coupled together with one operating as a motor and the other as a generator or load. Figure 6 shows a typical back-to-back test setup.

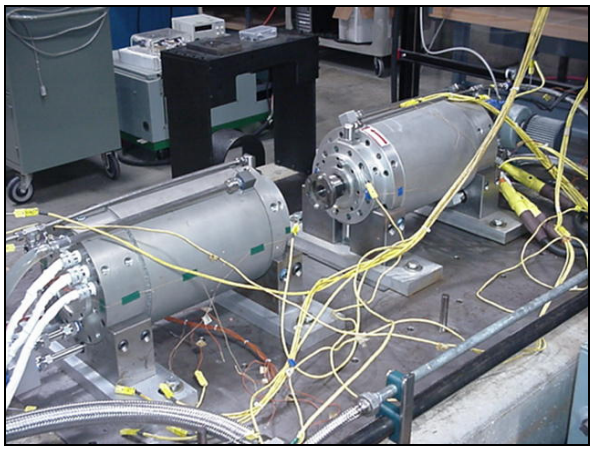

Figure 6 Back-to-back test setup.

By measuring the input power to the motor and output power from the generator, we can measure the total losses of the system that includes both units at various load conditions. Since the two machines are identical, we can calculate total loss for each machine without introducing significant errors by compensating for small differences in winding losses due to different operating current in each machine. For a more accurate assessment, a torque meter (if available) can also be used to directly measure the torque between the motor and generator.

4.2 Spin-Down Test

There is a relationship between the electromagnetic torque and the inertia torque as

$$T_{em} = J\frac{d\omega_r}{dt} + T_{damp} - T_{mech} \tag{19}$$

where T_{em} is the electromagnetic torque, T_{damp} is the damping torque in the direction opposite to rotation because of the friction, windage, and iron losses, T_{mech} is the externally applied mechanical torque in the direction of the rotor speed, and J is the rotor inertia.

Spin-down test is a method to measure the damping torque. When the motor is free spinning without externally applied mechanical torque and electromagnetic torque, equation (19) becomes

$$T_{damp} = -J\frac{d\omega_r}{dt} \tag{20}$$

Therefore, the motor losses can be calculated as

$$P_{loss} = -J \cdot \omega_r \frac{d\omega_r}{dt} \tag{21}$$

By measuring the initial speed versus time duration of the rotor from the initial speed to fully stop, the power loss can be calculated. When performing spin-down test, any armature electrical loops should be disconnected to ensure that the motor is spinning down freely without any braking effect. If there is output power during spin-down test, this power has to be considered in the calculation.

As an example, Figure 7 shows the measured spin-down time vs. rotor speed for a magnetic bearing supported high speed PM machine. The machine also produced output power of 140 W at 36,000 rpm, and 60 W at 8,000 rpm during spin-down. The inertia of the entirel rotating assembly is 0.68 kg-m^2. Figure 8 shows the calculated total no-load loss vs. rotor speed according to (21). The copper loss can be ignored in the calculation due to very low output power.

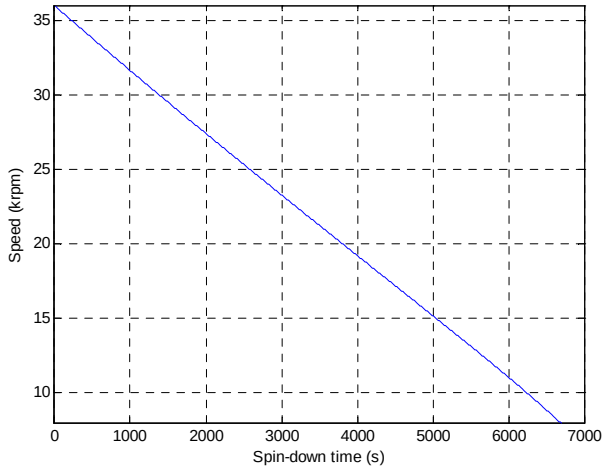

Figure 7 Measured machine spin-down time vs. rotor speed.

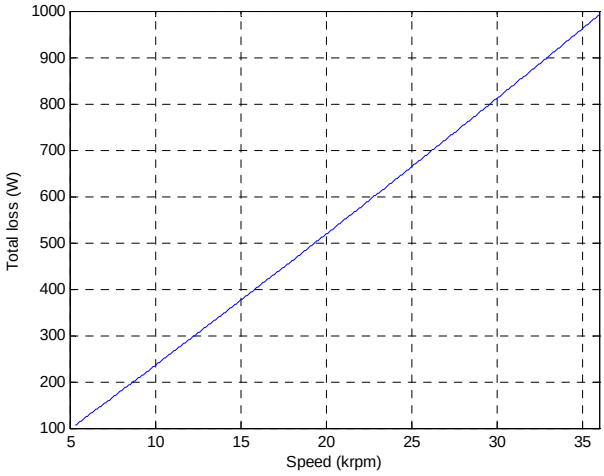

Figure 8 Calculated no-load total loss vs. speed.

4.3 Temperature Mapping and Correlation with Thermal Model

In this technique, the machine is well instrumented throughout with temperature sensors such as thermocouples or thermistors. Temperature measurements are then made for various operating conditions with different loads and speeds. A finite difference thermal model of the machine is also constructed with calculated losses assigned for various components of the machine. Figure 9 shows a typical machine thermal model.

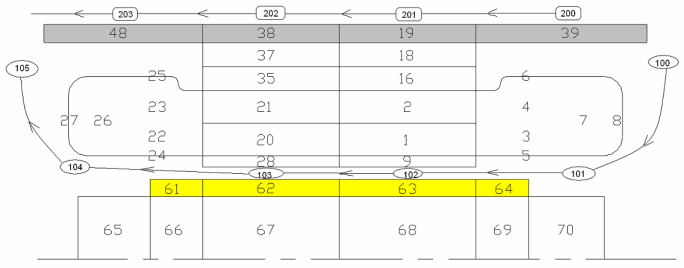

Figure 9 A typical lumped parameters thermal model of a PM machine.

By adjusting losses in the thermal model so that predicted temperatures match the measured results for various operating conditions, we can estimate roughly different loss components of the machine. Validity of this technique depends significantly on accuracy of the thermal model. Therefore this technique is often used as secondary check.

5 CONCLUSION

High speed PM machines possess many desirable attributes that make them attractive for direct drive applications such as microturbines. In this paper, we describe the losses in high-speed PM machines in details. A typical PM machine designed for microturbine application is presented and various verification methods are discussed. Accurate assessment of machine's losses is critical in doing system design tradeoffs as well as in predicting system performance and ensuring safe and reliable system operation.

6 REFERENCES

[1] Lammeraner, J., and Stafl, M., 1966, *Eddy Currents*, CRC. Press.

[2] Zheng, L., et. al., 2005, "Design of a super-high speed permanent magnet synchronous motor for cryogenic applications," *IEEE International Electric Machines and Drives Conferences, IEMDC'05*, San Antonio, TX, pp. 874-881.

[3] Hamdi, E. S., 1994, *Design of small Electrical Machines*, John Wiley & Sons Ltd.

[4] Mi, C., Slemon, G. R., and Bonert, R., 2003, "Modeling of Iron Losses of Permanent Magnet Synchronous Motors," IEEE Trans. Ind. Applic., **39** (3), pp. 734 -742.

[5] Binesti, D., and Ducreux, J. P., 1996, "Core losses and efficiency of electrical motors using new magnetic materials," *IEEE Trans. on Magnetics*, **32** (5), pp. 4887 - 4889.

[6] Smith, A.C., and Edey, K., 1995, "Influence of manufacturing processes on iron losses," *IEE Electrical Machines and Drives Conference*, pp. 77-81.

[7] Siemon, G. R., and Liu, X., 1990, "Core losses in permanent magnet motors," *IEEE Trans. Magnetics*, **26** (5), pp. 1653-1655.

[8] Emanuel, E., 1988, "The effect of nonsinusoidal excitation on eddy current losses in saturated iron," *IEEE Trans. Power Delivery*, **3** (2), pp. 662-671.

[9] Roshen, W., 2007, "Iron loss model for permanent magnet synchronous motors," *IEEE Trans. Magnetics*, **43** (8), pp. 3428-3434.

[10] Chari, M. V. K., 1980, "Finite element analysis of electrical machinery and devices," *IEEE Trans. Magnetics*, **16** (5), pp. 1014-1019.

[11] Shimoji, H., 2001, "Iron loss and magnetic fields analysis of permanent magnet motors by improved finite element method with E&S; model," *IEEE Transactions on Magnetics*, **37** (5), part 1, pp. 3526-3529.

[12] Jong, H. C. J. de, 1989, *AC Motor Design: Rotating Magnetic Fields in a Changing Environment*, Hemisphere Publishing Corporation.

[13] Vrancrik, J. E., 1968, "Prediction of Windage Power Loss in Alternators," *NASA-Langey TND-4849*, pp. 5-7.

[14] Becker, K.M., and Kaye, J., 1962, "Measurement of Diabetic Flowin annulus with an inner rotating cylinder," *ASME Journal of Heat Trasnsfer*, pp. 97-105.